ELSEVIER

Journal of Power Sources 112 (2002) 153–161

JOURNAL OF POWER SOURCES

www.elsevier.com/locate/jpowsour

Degradation behaviour of Al–Fe coatings in wet-seal area of molten carbonate fuel cells

JaeHo Jun[a,b,*], JoongHwan Jun[a], KyooYoung Kim[b]

[a]*Research Institute of Industrial Science and Technology, Pohang 790-600, South Korea*
[b]*Pohang University of Science and Technology, Pohang 790-784, South Korea*

Received 29 April 2002; accepted 14 June 2002

Abstract

The corrosion resistance of Al–Fe coatings increases as a protective $LiAlO_2$ layer forms. If, however, the Al–Fe coatings lack sufficient aluminium for maintaining this protective layer, the corrosion resistance of the coating is degraded by the growth of non-protective scales, such as $LiFeO_2$. In this study, the degradation behaviour of Al–Fe coatings is investigated in the wet-seal environment of molten carbonate fuel cells (MCFC). Al–Fe coated specimens with various amounts of aluminium in the range 8–70 at.% and bulk specimens of Fe–23.9 Al (at.%) are prepared. A corrosion test is performed in Li/K carbonate systems at 650 °C with a single-cell and an immersion test. Test results reveal that aluminium contents in the coatings should be higher than 25 at.% in order to form and maintain a protective $LiAlO_2$ layer. In addition to aluminium content, the influence of microstructural features on the degradation behaviour of Al–Fe coatings is discussed.

Keywords: Molten carbonate fuel cell; Al–Fe coating; Separator plate; Wet-seal corrosion

1. Introduction

Corrosion of separator plates in molten carbonate fuel cells (MCFC) is one of the major problems that hinder long-term performance of the cells. In particular, the wet-seal area of the separator plates—in direct contact with molten carbonate at 650 °C—undergoes the most severe corrosion [1]. The separator plates are usually made of stainless-steels, such as AISI 316L or AISI 310S. Previous studies have shown [1,2] that these stainless steels corrode very rapidly in wet-seal environments and therefore, cannot meet the durability requirement of 40,000 h for commercial MCFC applications.

It is an established fact that wet-seal materials should satisfy several requirements, which include high corrosion resistance, a high melting point, no electrical conductivity, and no dissolution in molten carbonate [3,4]. $LiAlO_2$ may be a suitable material to meet these requirements and, consequently, aluminium-containing alloys or aluminium coatings have been developed [5–10]. The aluminium source in alloys or coatings can react with molten carbonate and form a protective $LiAlO_2$ layer on the surface during MCFC operation. It has been reported, that a small addition of aluminium is beneficial for the corrosion resistance of stainless steels [5,6]. Nevertheless, the usage of aluminium-containing alloys is generally restricted by a limited amount of aluminium in alloys and poor mechanical properties. A more practical approach in developing suitable wet-seal material is the application of an aluminium coating followed by diffusion heat treatment. The heat treatment process is applied in order to transform pure aluminium coating layers into Al–Fe coating layers, which may contain various phases, such as Al_3Fe, Al_5Fe_2 and AlFe depending on the substrate material and the conditions of the heat-treatment process. Many researchers have reported that Al–Fe coatings have a high corrosion resistance against molten carbonate [7–10]. There are, however, still some doubts as to whether Al–Fe coatings maintain their protective function over an extended lifetime of 40,000 h [11,12]. Moreover, few studies have examined the lifetime of coated separators for application in MCFCs. In order to develop more reliable wet-seal materials which have sufficient corrosion resistance, a closer examination of the corrosion behaviour of Al–Fe coatings is required.

The purpose of this study is to establish a better understanding of the corrosion behaviour of Al–Fe coatings in the wet-seal area of the MCFC. Attention is directed towards

* Corresponding author. Tel.: +82-54-279-6452; fax: +82-54-279-6199.
E-mail address: jaeho@rist.re.kr (J. Jun).

0378-7753/02/$ – see front matter
PII: S0378-7753(02)00353-1

focusing on the influence of microstructure and aluminium content on the degradation behaviour of Al–Fe coatings. In this investigation, aluminium-coated separators are made by electron beam evaporation and are examined by operating single-cells at 650 °C to observe the corrosion behaviour of the coated separators. To confirm the results obtained from a single-cell test, various Al–Fe coated specimens and a bulk specimen are prepared for an immersion test, and the influence of aluminium content on the development of a stable $LiAlO_2$ layer is investigated in a Li/K carbonate melt at 650 °C.

2. Experimental procedures

2.1. Aluminium-coated separator

Commercial stainless-steel AISI 316L was used as a separator substrate, and the anode wet-seal area was selectively coated with aluminium by an evaporation process. A schematic diagram of the aluminium-coated separator plate, which has a cell area of 100 cm^2, is shown in Fig. 1. In the evaporation process, aluminium grains were placed in an alumina crucible and vaporised by heat generated from an electron-beam gun. The separator plate was held at 350 °C and the working pressure was maintained below 5×10^{-5} Torr. The deposition rate was controlled near 100 Å s^{-1}. The measured thickness of the aluminium coating layer was approximately 30 μm. Subsequently, the aluminium-coated separator was heat-treated at 700 °C for 3 h in an atmosphere of 20% H_2–80% N_2. After heat-treatment, the surface aluminium concentration was approximately 70 at.%.

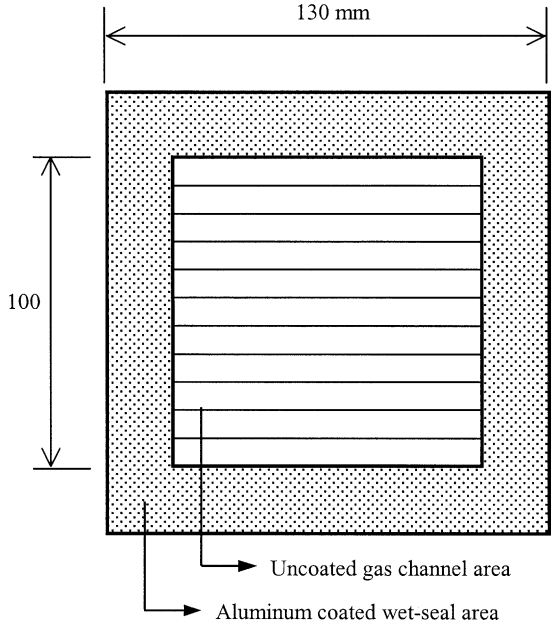

Fig. 1. Schematic diagram of aluminium-coated separator for MCFC single-cell.

2.2. Al–Fe coated- and Al–Fe bulk-specimens

Four Al–Fe coated specimens containing various amounts of aluminium (viz. Fe–8 Al, Fe–15 Al, Fe–25 Al and Fe–36 Al (at.%)) were prepared by using a single-source evaporation method [13]. In order to make a comparison with the coated specimens, a cast specimen of Fe–23.9 Al (at.%) alloy was prepared, cast by arc melting, followed by homogenising treatment at 1000 °C for 5 h.

2.3. Single-cell test and immersion test

In the single-cell test, the aluminium-coated separator was put in a single-cell, which was operated at 650 °C under a constant load of 150 mA cm^{-2}. For the gas, 72% H_2–18% CO_2–10% H_2O and 70% air–30% CO_2 were supplied for the anode and the cathode, respectively. A total of 62 mol% Li_2CO_3–38 mol% K_2CO_3 in a $LiAlO_2$ matrix served as the electrolyte. After conducting the single-cell test for 2500 h, the corrosion products and the coating layer were analysed by scanning electron microscopy (SEM), back-scattered electron microscopy (BEM), X-ray deflection (XRD), and electron probe microanalysis (EPMA). The corrosion kinetics of the aluminium-coated separator were determined by measuring scale thickness in metallographic cross-sections. In addition to the single-cell test, an immersion test was conducted to investigate the effect of aluminium content on the corrosion behaviour of Al–Fe coatings. The Al–Fe coatings and the Fe–23.9 Al (at.%) alloy were fully immersed in a eutectic Li/K carbonate melt (62 mol% Li_2CO_3–38 mol% K_2CO_3) at 650 °C. Following the immersion test, the corrosion products formed on the coated specimens and the bulk specimen were identified. The corrosion kinetics of the Fe–23.9 Al alloy was also examined by measuring weight changes with respect to immersion time.

3. Results and discussion

3.1. Degradation behaviour of aluminium-coated separator (single-cell test)

The single-cell test was performed to explore the corrosion behaviour of the aluminium-coated separator in the MCFC wet-seal environment. The scale thickness data of the uncoated separator (AISI 316L) and the aluminium-coated separator in terms of operation time are shown in Fig. 2. It was clearly demonstrated that the corrosion rate of the aluminium-coated separator was much lower than that of uncoated versions. After 2500 h of operation time, the scale thickness of the uncoated separator was approximately 50 μm, while that of the aluminium-coated separator was approximately 8 μm. The aluminium-coated separator formed only $LiAlO_2$ as its corrosion product, whereas two different corrosion products formed on the uncoated separator. Both products consisted of two layers, an outer

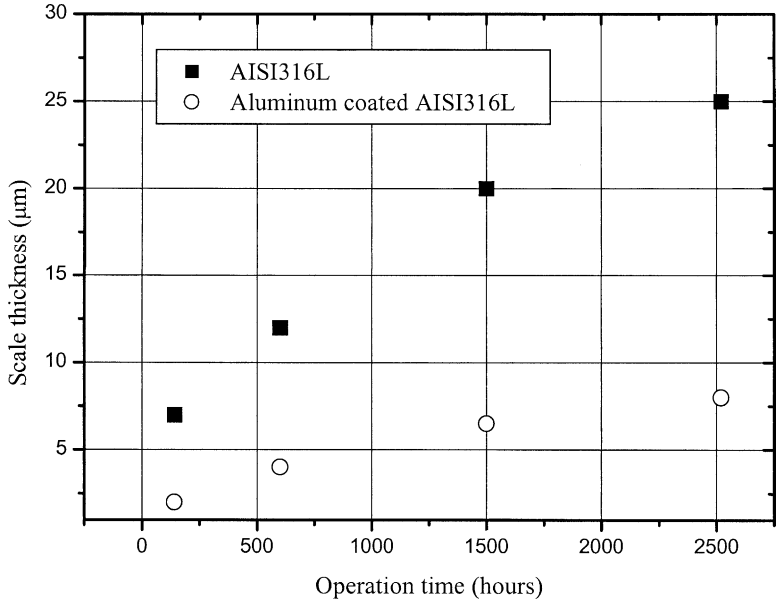

Fig. 2. Scale thickness of AISI 316L and aluminium-coated AISI 316L after various operation times with single-cells.

layer of $LiFeO_2$ and an inner layer of $LiCrO_2$. Test results confirmed that an aluminium coating enhances the corrosion resistance of AISI 316L by the formation of a protective $LiAlO_2$ layer. It is well known, that aluminium is oxidised to form stable oxides, such as $LiAlO_2$ or Al_2O_3 in molten Li/K carbonates. Possible oxidation reactions of the aluminium are as follows [14]:

$$Al + Li^+ + 2CO_3{}^{2-} \rightarrow LiAlO_2 + 2CO_2 + 3e^- \quad (1)$$

$$2Al + 3O^{2-} \rightarrow 2Al_2O_3 + 6e^- \quad (2)$$

where the oxide ions are supplied by the dissociation of carbonate ion ($CO_3{}^{2-} \rightarrow CO_2 + O^{2-}$), or by the gas dissolved in the molten carbonate.

As described above, the aluminium coating provided higher corrosion resistance. On the other hand, if the coating layer (i.e. Al–Fe phases) lacks sufficient aluminium content for the formation of a stable $LiAlO_2$ layer, it may form non-protective iron oxides. This is due to fact that $LiAlO_2$ formation on Al–Fe coatings is contingent on aluminium content. This possibility is shown in Fig. 3. First of all, the coating layer in the region marked as C1 in Fig. 3 is characterised by uneven scale morphology that results from localised attack of the coating surface and growth of corrosion products inside the coating layer. Such corrosion behaviour at the surface is thought to be associated with rough surface texture, inhomogeneous composition distribution, and microstructural defects. A back scattered election image

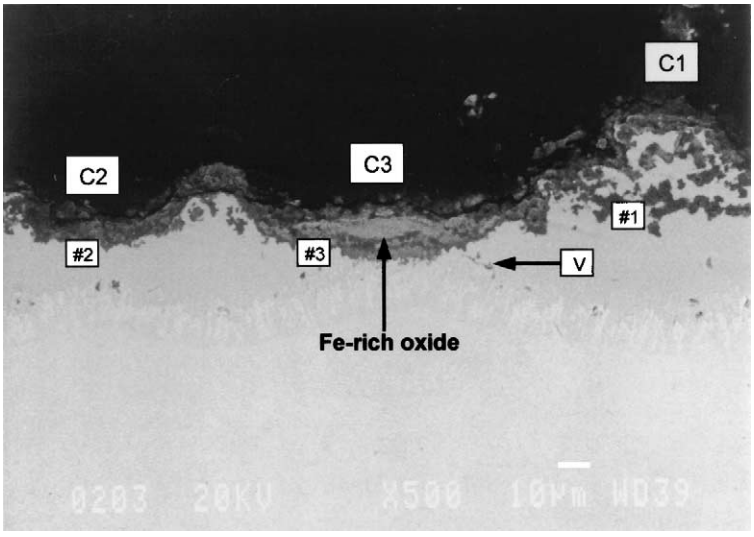

Fig. 3. Cross-sectional image of aluminium-coated separator after 2500 h of operation, showing a corrosion sequence of coating layer degradation.

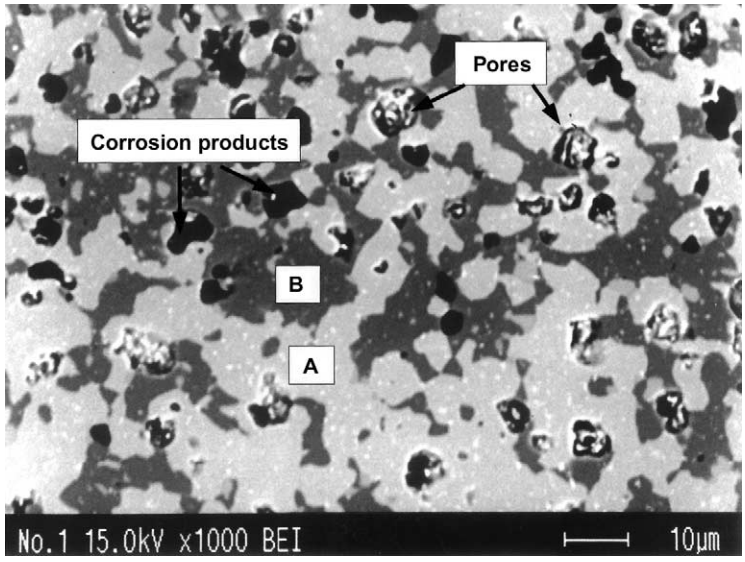

Fig. 4. Surface image of sample polished to approximately 10 μm from top surface of aluminium-coated separator after 2500 h operation.

is shown in Fig. 4 of the sample that was polished to about 10 μm from the top surface of the aluminium-coated separator after 2500 h of operation. Corrosion products are still observed even inside the coating layer, which appears to be connected with the presence of pores. In addition, different shades in the image (Fig. 4) indicate that the surface lacks homogeneous composition. In fact, the chemical compositions of point A of and point B were analyzed by EDS as 47.2 Al–41.1 Fe–7.5 Cr–4.2 Ni and 64.9 Al–30.1 Fe–3.8 Cr–1.2 Ni (at.%), respectively, which may provide an indication that the top part of the coating layer is mixed with FeAl phase and Fe_2Al_5 phase. These surface properties are dependent on aluminium-coating methods and the diffusional interaction between coating and substrate during the heat-treatment process and MCFC operation [9,10,15].

Due to the coating surface features discussed above, carbonate salt erodes the coating layer in region C1 (Fig. 3), which results in the loss of its outer portion. Consequently, this could lead to a thin coating layer like region C2 in Fig. 3. Because the coating layer in region C2 is thinner than normal coating layers, the aluminium surface concentration is certainly lower. Chemical compositions at points #1 to #3 in Fig. 3 were measured by EDS, with results listed in Table 1. The aluminium concentration is 21.2 at.% at point #3 and 41.5 at.% at point #1. It is necessary for the coating layer to retain a sufficient content of aluminium to form a protective scale, such as $LiAlO_2$, as well as to maintain growth during the coating lifetime. In this respect, region C2 may act as a position where iron oxides can be formed instead of $LiAlO_2$. This is shown in region C3 in Fig. 3. As corrosion progresses, the iron oxides increase in size, and oxygen can even penetrate through the scale and coating layer into the substrate, as shown in Fig. 5.

Table 1
EDS quantitative analysis at sites of #1, #2 and #3 in Fig. 3 after 2500 h operation of single-cell (at.%)

Position (#)	Al	Fe	Cr	Ni
1	41.5	46.4	8.2	3.9
2	34.3	50.0	8.8	6.9
3	21.2	52	12.6	14.3

On the other hand, voids are observed primarily at the interface between the coating layer and the substrate, as shown in Figs. 3 and 5. Such voids are able to influence the corrosion behaviour of the coating layer, especially pitting corrosion that occurs in the final stage of corrosion degradation. In fact, the void marked V (Fig. 3) can act as a rapid diffusion site for lithium and oxygen ions and result in accelerated degradation of the coating layer, as shown in Fig. 5. Examples of the void formation have also been found in other studies [16,17], and such voids might be generated by means of the Kirkendall effect [17,18]. According to Fujimoto et al. [16], the area fraction of voids increases over time and can reduce the corrosion resistance of the Al–Ni coating layer in MCFC wet-seal environments.

In order to understand better the degradation behaviour of the coating layer, an investigation of the phases formed in the coating layer was conducted over 2500 h. Two isothermal sections at 650 °C, based on Al–Fe–Cr [19] and Al–Fe–Ni ternary phase diagrams [20] are shown in Fig. 6a and b, respectively. The chemical compositions of points #1 to #3 (Fig. 3) are expressed by omitting Ni in the Al–Fe–Cr phase diagram and omitting Cr in the Al–Fe–Ni phase diagram. First, point #1, which corresponds to one of the upper parts of the coating layer (Fig. 3), is located in the two-phase field, α2(FeAl) and (Cr, αFe), in the ternary Fe–Al–Cr system or in the one phase field, $\alpha((Fe_xNi_{1-x})Al_{1-y})$, in the ternary Fe–Al–Ni system. Therefore, it is concluded that the site consists of an FeAl phase with a small amount of nickel and a (Cr, αFe) phase. Second, point #2, which corresponds to one of the lower parts of the coating layer (Fig. 3), is also found

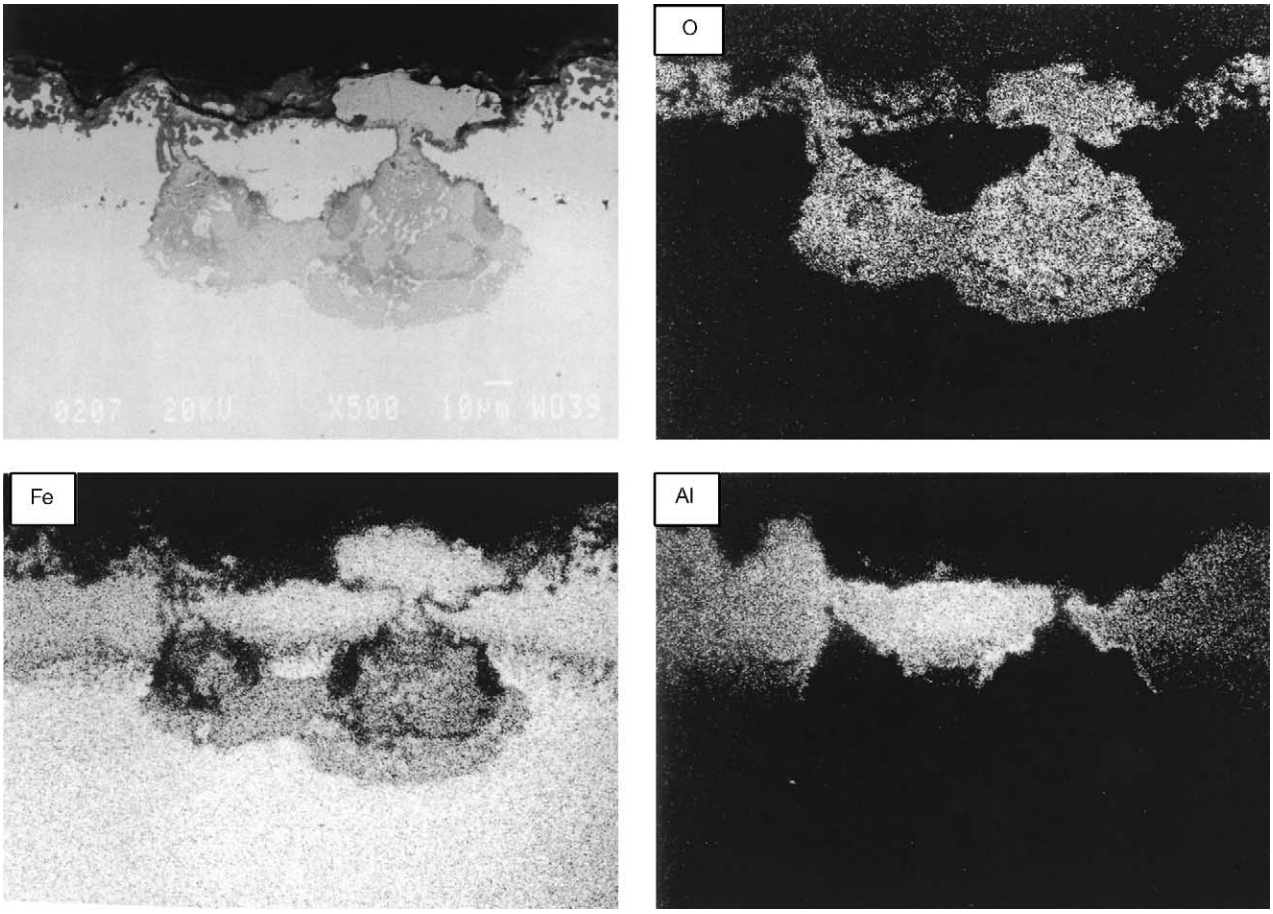

Fig. 5. Cross-sectional image and EPMA mapping of Al, Fe, and O for aluminium-coated separator after 2500 h of operation, showing pitting corrosion.

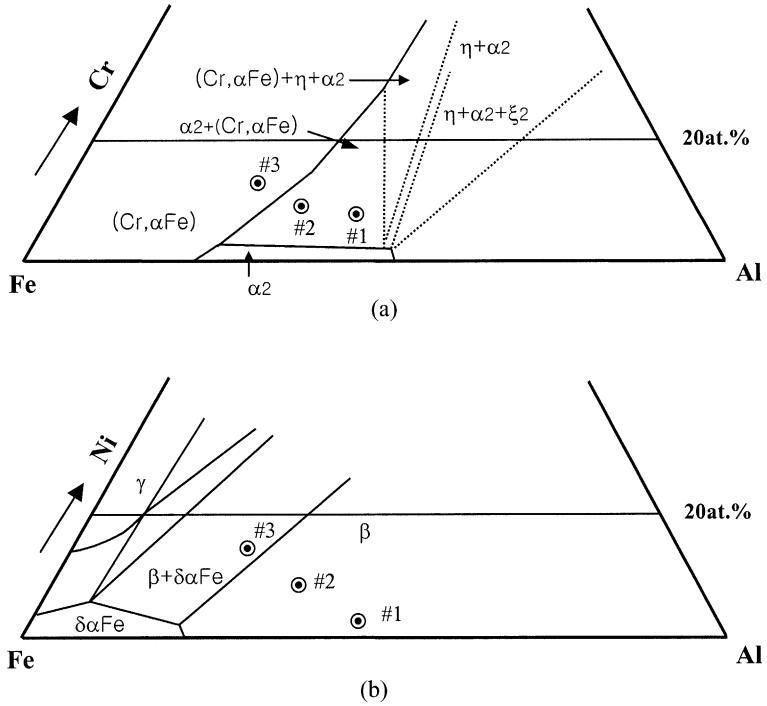

Fig. 6. Phase diagrams of Al–Fe–Cr and Al–Fe–Ni systems at 650 °C. (a) Al–Fe–Cr phase diagram; (b) Al–Fe–Ni phase diagram.

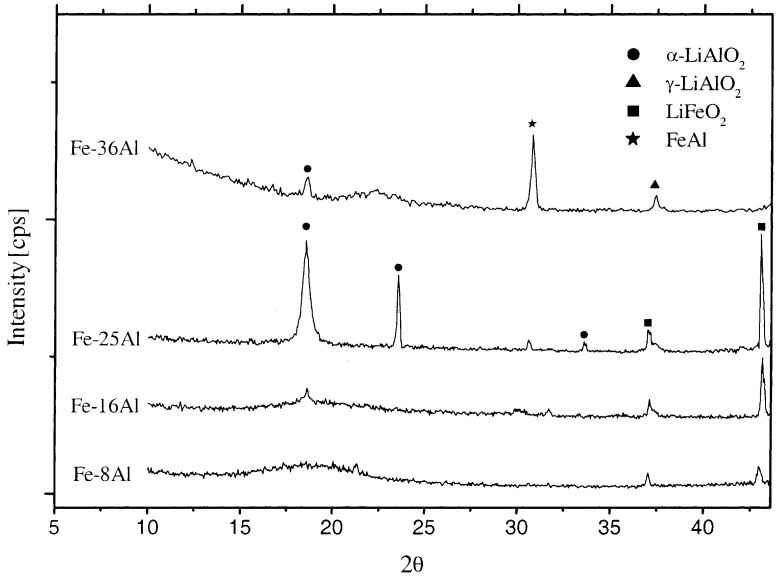

Fig. 7. XRD analysis of various Fe–Al coated specimens after immersion in Li/K carbonate melt at 650 °C for 24 h.

in the same field as point #1, but shifts near a new Fe-side phase field due to the decrease in aluminium content. Finally, point #3, in the vicinity of where iron-rich oxide was observed, as shown in Fig. 3a, lies in the one-phase field (Cr, αFe) in the Al–Fe–Cr system or in the two-phase field β+ δαFe phase in the Al–Fe–Ni system. According to the phase study of the coating layer after 2500 h, it is noteworthy that the phases become more complex as the coating compositions are changed. Considering, both the corrosion resistance and the microstructural stability of the coating layer, it is desirable for the coating layer to keep one phase such as β, which has a wide solubility range for Fe, Ni and Cr. All things considered, however, the fact is that the coating layer consists of either a mixture of α2 and (Cr, αFe) in the ternary Al–Fe–Cr system or α and δαFe in the ternary Al–Fe–Ni system. Regarding local corrosion, such complex phases could be reflected in the degradation mechanism of the coating layer illustrated in Figs. 3 and 5.

3.2. Influence of aluminium content (immersion test I)

An immersion test was carried out to examine the critical aluminium content required for the formation of a continuous protective $LiAlO_2$ layer in molten carbonate. The

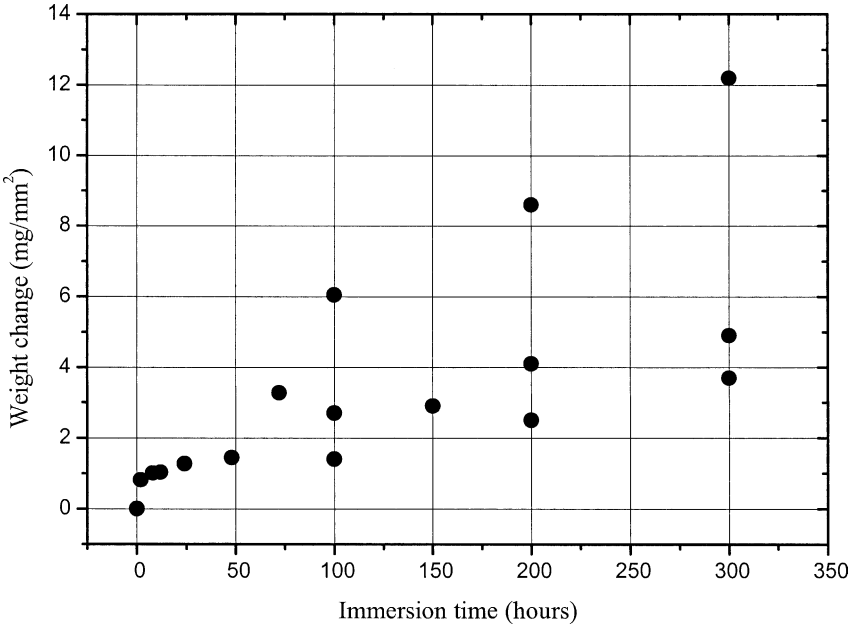

Fig. 8. Weight change versus immersion time of a Fe–23.9 Al alloy specimen in Li/K carbonate melt at 650 °C.

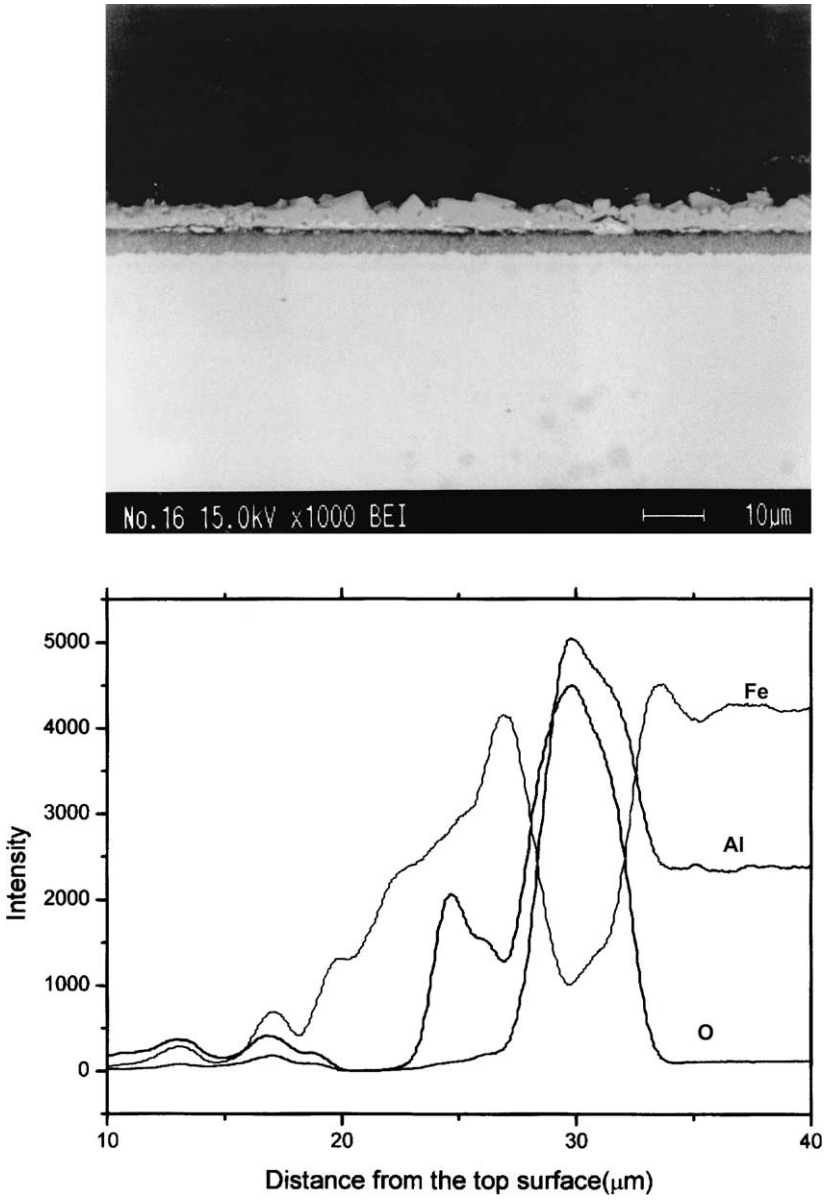

Fig. 9. Cross-sectional morphology and EDS line profiles across scales formed on a Fe–23.9 alloy specimen after immersion in Li/K carbonate melt for 16 h at 650 °C.

results of XRD analysis of Fe–Al coated specimens after a 24 h immersion test in the eutectic Li/K carbonate melt at 650 °C are shown in Fig. 7. The XRD results reveal that the Fe–8 Al specimen shows sharp $LiFeO_2$ peaks and broad and weak $LiAlO_2$ peaks. The sharp $LiAlO_2$ peaks began to appear in the Fe–18 Al specimen. The intensities of $LiAlO_2$ peaks increased with increase in aluminium content in the Al–Fe coatings. The corrosion products of the Fe–25 Al coated specimen consist of $LiFeO_2$, and $LiAlO_2$. In addition, only $LiAlO_2$ peaks are observed for the Fe–36 Al specimen, which indicates that the $LiAlO_2$ scale is formed completely on the surface. The test results show that the aluminium contents required for the formation of a stable and protective $LiAlO_2$ in the eutectic Li/K carbonate melt at 650 °C should be higher than 25 at.%.

Many studies have been conducted on the oxidation behaviour of iron–aluminum alloys in gaseous atmospheres and have revealed that a certain percentage of aluminium is required to form completely protective Al_2O_3 scales [21–23]. For example, according to Pint et al. [21], the critical aluminium content required to form completely protective Al_2O_3 scales in air is approximately 20, 18, 14 at.% at 600, 700 and 800 °C, respectively. Few studies have been reported on the corrosion behaviour of aluminium–iron alloys, although that of iron and iron-based alloys has been extensively studied in molten carbonate systems [24–28]. Moreover, the corrosion behaviour in the presence of molten carbonate salt differs from that in a simple gaseous atmosphere. With regard to the effect of aluminium content, other investigations of the corrosion behaviours of Fe–Al

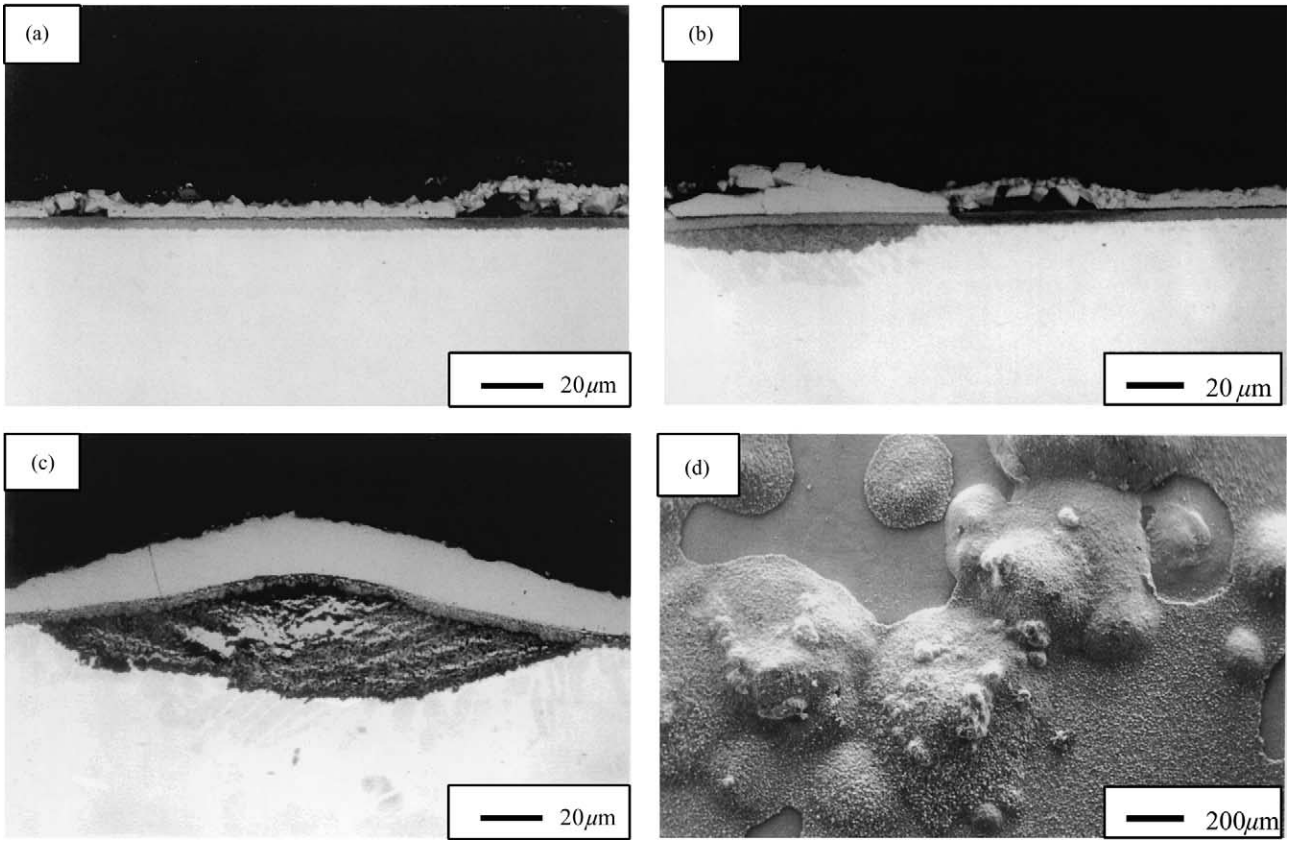

Fig. 10. Cross-sectional and surface morphologies of scales formed on a Fe–23.9 Al alloy specimen after immersion test Li/K carbonate melt at 650 °C for: (a) 24 h; (b) 48 h; (c) 72 h and (d) 300 h.

and Ni–Al alloys in wet-seal environments have been surveyed. Zeng et al. [29] reported that an Fe–Al–B alloy containing approximately 40 at.% aluminium formed a three-layer scale which contained external $LiFeO_2$, intermediate iron oxides, and inner Al_2O_3 after immersion in a Li/K carbonate melt at 650 °C for 100 h. Frangini et al. [30] pointed out that oxide-dispersion strengthened (ODS) Fe–Al alloys containing approximately 38 at.% Al formed a thin continuous and protective aluminum-oxide layer, which maintains a long-term corrosion resistance in a Li/K carbonate melt, but a high CO_2 gas content may be detrimental to corrosion resistance due to pitting corrosion along the grain boundaries that correspond to the position of the yttria particles. In addition, Vossen et al. [14] examined the corrosion behaviour of Ni–Al alloys with aluminium contents of 2–50 at.% in a Li/K carbonate melt by electrochemical tests. According to their study [14], continuous $LiAlO_2$-scales are formed only when the aluminium content is very high (approximately 50 at.%), while NiO and aluminium oxides are formed on alloys containing 20 at.% aluminium.

3.3. Corrosion behaviour of Fe–23.9 Al alloy (immersion test II)

A bulk Fe–23.9 Al (at.%) specimen was selected with the aim of not only examining its corrosion behaviour in molten carbonate, but also verifying the test result of the Fe–25 Al coated specimen. The Fe–25 Al coated specimen could not form an external $LiAlO_2$ in the eutectic Li/K carbonate melt, as shown Fig. 7. Weight-gain curves for the cast specimen of Fe–23.9 Al in the eutectic melt at 650 °C are shown in Fig. 8. Scale growth showed parabolic kinetics up to about 50 h. With further reaction, however, the Fe–23.9 Al alloy starts to corrode rapidly with larger weight gain, which suggests a lack of development of a stable protective film. Scattered data are also shown in Fig. 8 and are probably due to spalled scales. The cross-sectional morphology and EDS line profiles across scales which formed on the Fe–23.9 Al alloy for 16 h are shown in Fig. 9. The Fe–23.9 Al alloy formed a two-layer scale, composed of a porous exterior phase and a dark inner phase. One Fe-peak, one Al-peak and two distinguishable O-peaks were observed by EDS analysis, and correspond to iron-rich and aluminium-rich oxides, respectively, on the surface. Compared with the results of the XRD analysis, scales formed on the Fe–23.9 Al bulk specimen might be $LiFeO_2$ and inner aluminium-rich oxides during the initial stage. In spite the fact that the scales on the Fe–25 Al alloy after 16 h contained an aluminium-rich oxide layer at the interface between $LiFeO_2$ and the substrate, the Fe–23.9 Al alloy displays breakaway behaviour with rapid weight gain after about 50 h.

The exact corrosion mechanism on the Fe–23.9 Al alloy is not clear, but an examination of scale morphology (Fig. 10) reveals that inner aluminium-rich oxides do not maintain a reliable protective function, which implies that aluminium content is insufficient to form a protective layer. After a short initial time, outer $LiFeO_2$ scales, which are porous and have many defects (Fig. 10a), allow lithium or oxygen ions to approach freely the inner aluminium-rich oxide layer and penetrate further into the substrate (Fig. 10b). This may be because the inner layer is not able to prevent lithium or oxygen ions from penetrating through defects in the outer porous scales. This continued process results in swollen and convex type products beneath the inner continuous scales and cracks in the outer scales (Fig. 10c). The corrosion products are composed of a mixture of iron and aluminium oxides. Eventually, the scale surface morphology which formed on the Fe–23.9 Al alloy in the eutectic melt displays characteristics of discontinuous outer scales, random formation of nodule-like scales, and partial spalling of the scales, as shown in Fig. 10d. These features result in the mass-gain behaviour shown in Fig. 8.

4. Conclusions

The degradation behaviour of Al–Fe coatings has been investigated in a MCFC wet-seal environment at 650 °C using a single-cell test and an immersion test. In the single-cell test, the aluminium-coated separator exhibits higher corrosion resistance than the uncoated separator due to the formation of a protective $LiAlO_2$ layer on the surface. Degradation of the coating layer is initiated, however, by localised corrosion, which leads to a lack of aluminium concentration. Eventually, non-protective iron oxides form instead of $LiAlO_2$, and pitting corrosion takes place. This corrosion behaviour appears to be influenced by inhomogeneous microstructures, such as complex phases and voids, as well as by a decrease in aluminium concentration across the coating layer because of the interdiffusion of aluminium and iron. In the immersion test, Al–Fe coated specimens which contain aluminium from 8 to 25 at.% and bulk Fe–23.9 Al (at.%) alloy formed predominantly $LiFeO_2$ scales, and corrode with a large weight gain, while the Al–36 Fe coating develops external $LiAlO_2$ scales. Immersion test results indicate that the critical aluminium level required for formation of a protective $LiAlO_2$ layer in a Li/K carbonate melt at 650 °C lies between 25 and 36 at.%.

References

[1] J.R. Selman, in: L.J.M.J. Blomen, M.N. Mugerwa (Eds.), Fuel Cell Systems, Plenum Press, New York, 1993.
[2] R.A. Donado, L.G. Marianowski, H.C. Maru, J.R. Selman, J. Electrochem. Soc. 131 (1984) 2541.
[3] M. Keijzer, K. Hemmes, P.J.J.M. Van Der Put, J.H.W. de Wit, J. Schoonman, Corrosion Sci. 39 (1997) 483.
[4] R.A. Donado, L.G. Marianowski, H.C. Maru, J.R. Selman, J. Electrochem. Soc. 131 (1984) 2535.
[5] G. Lindbergh, B. Zhu, Electrichim. Acta 46 (2001) 1131.
[6] M. Sasaki, S. Ohta, M. Asno, N. Igata, Corrosion Eng. 45 (1996) 231.
[7] C. Yuh, R. Johnsen, M. Farooque, H. Maru, in: D. Shores, H. Mau, I. Uchida, J.R. Selman (Eds.), Proceedings of the Symposium on Molten Carbonate Fuel Cell Technology, The Electrochemical Society, 1993, p. 158.
[8] K. Matsumoto, A. Matsuoka, K. Nakagawa, Denki Kagaku Jpn. 66 (1998) 537.
[9] J.E. Indacochea, I. Bloom, M. Krumpelt, T.G. Benjamin, J. Mater. Res. 13 (1998) 1834.
[10] C.Y. Yuh, P. Singh, L. Paetsch, H.C. Maru, in: Proceedings of the Symposium on Corrosion'1987, NACE Paper no. 276, NACE, 1987.
[11] Y. Kawabata, N. Fujimoto, M. Yamamoto, T. Nagoya, M. Nishida, J. Power Sources 86 (2000) 324.
[12] A. Agüero, F.J. García de Blas, M.C. García, R. Muelas, A. Román, Surf. Coat. Technol. 146/147 (2001) 578.
[13] S. Schiller, U. Heisig, S. Panzer, Electron Beam Technology, Wiley, New York, 1982.
[14] J.P.T. Vossen, R.C. Makkus, A.H.H. Jansen, J.H.W. de Wit, Mater. Corrosion 48 (1997) 228.
[15] J.H. Jun, Joong H. Jun, J.C. Shin, K.Y. Kim, J. Corrosion Sci. Soc. Korea 27 (1998) 525.
[16] N. Fujimoto, M. Yamamoto, T. Nagoya, J. Power Sources 71 (1998) 231.
[17] M. Yamamoto, N. Fujimoto, Y. Uematsu, T. Nagoya, Nisshin Steel Tech. Rep. Jpn. 73 (1996) 18.
[18] P. Shewmon, Diffusion in Solids, TMS, Pennsylvania, 1989.
[19] V.G. Rivin, G.V. Raynor, Int. Met. Rev. 25 (1980) 139.
[20] V.G. Rivin, G.V. Raynor, Int. Met. Rev. 25 (1980) 79.
[21] B.A. Pint, J. Leibowitz, J.H. DeVan, Oxid. Met. 51 (1999) 181.
[22] P. Tomaszewicz, G.R. Wallwork, Oxid. Met. 19 (1983) 165.
[23] R. Prescott, M.J. Graham, Oxid. Met. 38 (1983) 73.
[24] D.A. Shores, P. Singh, in: J.R. Selman, T.D. Claar (Eds.), Proceedings of the Symposium on Molten Carbonate Fuel Cell Technology, The Electrochemical Society, 1984, p. 271.
[25] H.S. Hsu, J.H. DeVan, M. Howell, J. Electrochem. Soc. 134 (1987) 3038.
[26] M. Spiegel, P. Biedenkopf, H.J. Grabke, Corrosion Sci. 39 (1997) 1193.
[27] P. Biedenkopf, M. Spiegel, H.J. Grabke, Electrochim. Acta 44 (1998) 683.
[28] B. Zhu, G. Lindbergh, A. Simonsson, Corrosion Sci. 41 (1999) 1515.
[29] C.L. Zeng, W. Wang, W.T. Wu, Oxid. Met. 53 (2000) 289.
[30] S. Frangini, Oxid. Met. 53 (2000) 139.